Journal of Magnetic Resonance 209 (2011) 83–87

Contents lists available at ScienceDirect

Journal of Magnetic Resonance

journal homepage: www.elsevier.com/locate/jmr

Communication

A Bayesian approach to characterising multi-phase flows using magnetic resonance: Application to bubble flows

D.J. Holland [a,*], A. Blake [b], A.B. Tayler [a], A.J. Sederman [a], L.F. Gladden [a]

[a] Department of Chemical Engineering and Biotechnology, University of Cambridge, Pembroke Street, Cambridge CB2 3RA, United Kingdom
[b] Microsoft Research Cambridge, 7 J.J. Thomson Avenue, Cambridge CB3 0FB, United Kingdom

ARTICLE INFO

Article history:
Received 20 August 2010
Revised 9 November 2010
Available online 17 December 2010

Keywords:
Bayesian analysis
Multi-phase flows
Sparse *k*-space
Bubble size distributions
Magnetic resonance

ABSTRACT

Magnetic Resonance (MR) imaging is difficult to apply to multi-phase flows due to both the inherently short T_2^* characterising such systems and the relatively long time taken to acquire the data. We develop a Bayesian MR approach for analysing data in *k*-space that eliminates the need for image acquisition, thereby significantly extending the range of systems that can be studied. We demonstrate the technique by measuring bubble size distributions in gas–liquid flows. The MR approach is compared with an optical technique at a low gas fraction (~2%), before being applied to a system where the gas fraction is too high for optical measurements (~15%).

1. Introduction

Magnetic resonance (MR) is being increasingly applied to study multi-phase flows due to its ability to study optically opaque systems non-invasively. However, MR is an inherently slow technique with conventional imaging approaches requiring several minutes to acquire an image. A variety of fast imaging techniques are available [1–3], however these are still not quick or robust enough to study multi-phase flows which are characterised by rapid temporal variations, high shear rates and short relaxation times. This paper presents a new method of characterising multi-phase flows by re-posing the MR experiment as a Bayesian analysis problem that does not require image acquisition. Such an approach is advantageous for dynamic systems and could also be applied to low sensitivity portable MR systems. The procedure is developed and demonstrated for sizing gas bubbles in liquid flows.

Accurate measurement of bubble size is critical to improving our understanding of fundamental physical phenomena in multi-phase flows including turbulent drag, bubble coalescence, and heat transfer. However, the sizing of bubbles, particularly in high volumetric gas fraction flows, remains challenging. Measurements are currently made using optical, electrical, and light scattering techniques, amongst others [4–6]; these techniques have their limitations. Invasive techniques distort the local bubble size and shape. Non-invasive techniques are limited to low gas fraction ($\lesssim$5%) systems or near wall observations because of the increased light scattering by dense bubble swarms and interference effects between neighbouring bubbles. The Bayesian approach developed in this work is applicable to high gas fraction measurements (up to ~50%), and thus enables measurements of systems that were previously impossible to study.

Bayesian analysis has previously been used in a variety of MR applications [7–10]. It has been shown to improve the recovery of an MR spectrum from noisy data [7] and to improve the accuracy of flow measurements by enabling a sparse sampling procedure to be used [9]. In this work we exploit both these advantages of Bayesian analysis to enable measurements of the bubble size distribution in a dynamic system.

The approach used is derived from texture analysis concepts in image processing [11] and extends previous approaches for analysing MR data [12] to provide quantitative measurements in dynamic systems. The signal measured using MR, $S(k)$, is governed by:

$$S(k) = \int \rho(x) \exp(i2\pi kx) dx, \tag{1}$$

where $\rho(x)$ defines the image (e.g. liquid map), x corresponds to the spatial position and $k = \gamma(2\pi)^{-1} \int G_x(t)dt$, where γ is the gyromagnetic ratio and $G_x(t)$ describes the strength of the magnetic field gradient in the x-direction as a function of time, t. Thus, the signal, $S(k)$, and image, $\rho(x)$, are mutually conjugate Fourier pairs; hence by controlling the gradient strength as a function of time it is possible to sample any point in the spatial frequency domain of the image, commonly referred to in MR literature as *k*-space [13].

* Corresponding author.
E-mail address: djh79@cam.ac.uk (D.J. Holland).

1090-7807/$ - see front matter © 2010 Elsevier Inc. All rights reserved.
doi:10.1016/j.jmr.2010.12.003

In conventional MR, an image of the system is obtained by measuring a signal in k-space and then taking a discrete Fourier transform of these data. This image would subsequently be analysed to obtain the desired information, for example a bubble size distribution. However, multi-phase flows will often change over a time scale less than that required to acquire an image, leading to misregistration artefacts in the image that make the subsequent analysis challenging, inaccurate and frequently impossible.

In the Bayesian approach proposed in this paper, a likelihood function is developed relating the measured signal, $S(k)$, to the state of the system θ (e.g. the bubble size distribution). This eliminates the conventional imaging requirement that the system is stable for the duration of the acquisition, requiring only that θ is constant during the experiment. In this specific case of a bubble size distribution, the size and location of individual bubbles will change over a time scale of the order of a few milliseconds. However, the overall distribution of bubble sizes will remain stable over time, as it is determined by only the fluid properties, system design and operating conditions [14]. Therefore, a system that cannot be studied by image acquisition can be studied using a Bayesian methodology. The Bayesian approach reported here enables the characterisation of the size distribution of approximately spherical objects in multiphase systems. Therefore, in addition to the example of bubble sizing reported here, this same analysis could be applied to, for example, emulsion droplet sizing, droplet sizing of sprays, and the determination of pore size in porous media. The present case study was selected because the measurement of bubble size distributions in gas–liquid flows above a gas fraction of 5% cannot be made by optical techniques and represents a significant measurement challenge. We develop the technique and present results from numerical simulations of bubble size distributions with both ideal and noisy data. Numerical simulations suggest that the technique is applicable up to a gas fraction of 50%. We then compare experimental measurements of the bubble size distribution at low gas fraction (~2%) with an optical technique, before presenting measurements of the bubble size distribution at a gas fraction of ~15%, which is in excess of that which can be measured optically.

2. Model development

In Bayesian analysis the state of a system θ is inferred from a set of observations $\hat{y}$ from the posterior probability density function $p(\theta|\hat{y})$:

$$p(\theta|\hat{y}) \propto p(\hat{y}|\theta)p(\theta), \tag{2}$$

where $p(\hat{y}|\theta)$ is the likelihood function and $p(\theta)$ incorporates prior knowledge. In this work we are attempting to determine the size distribution of bubbles, which corresponds to θ, given a set of measurements, $\hat{y}$, of the signal intensity in k-space. In the approach described here, we assume a functional form for the size distribution and estimate the parameters of that distribution. Thus, if the radius of an individual bubble is r, then we characterise the distribution of r by modelling it using two parameters, the mean radius $\bar{r}$ and a standard deviation σ_r. These two parameters describe the state of the system θ, which we obtain as $p(\theta|\hat{y})$. We present results for two cases: (i) bubbles of a single size, i.e. $\sigma_r = 0$ and $r_j = \bar{r}$ for all bubbles j and (ii) a bubble size distribution given by a log-normal distribution, where the log-normal distribution is defined by:

$$p(r,\mu,\sigma_\mu) = \frac{1}{r\sigma_\mu\sqrt{2\pi}}\exp\left(-\frac{(\ln r-\mu)^2}{2\sigma_\mu^2}\right), \tag{3}$$

and the parameters μ and σ_μ uniquely define the mean $\bar{r} = \exp\left(\mu+\sigma_\mu^2/2\right)$ and variance $\sigma_r^2 = \bar{r}^2\left(\exp\left(\sigma_\mu^2\right)-1\right)$ of the distribution. We use a log-normal distribution as this is observed empirically [4,5]. In each case, the calculated posterior distribution characterises the probability distribution for the parameters $\bar{r}$ and σ_r.

The likelihood function is determined by considering how the signal intensity varies in k-space given a particular distribution of bubble sizes and bubble shape. We begin by formulating a 1D image $f(x)$ which comprises the projection of N bubbles onto the x-axis. The projection of each individual bubble is defined by a function $h(r,x)$, where r is the characteristic size of the bubble and x is the spatial coordinate. Then, defining the Fourier transforms of $f(x)$ and $h(r,x)$ as $F(k)$ and $H(r,k)$, respectively, the signal measured by MR obeys:

$$F(k) = \sum_{j=1}^{N} H(r_j,k)\exp(-i2\pi k x_{c,j}), \tag{4}$$

where $x_{c,j}$ is the location of the centre of the jth bubble and use has been made of the linearity and shift invariance of the Fourier transform. As an example, Fig. 1 shows (a) $f(x)$ for a simulation of 30 identical spherical bubbles and (b) the corresponding magnitude of $F(k)$, the discrete Fourier transform of these data. Assuming $\{x_{c,j}\}$ is independent and identically distributed, then for a given k, the expected $F(k)$ is 0, i.e. $E(F(k)) = 0$ and

$$E(|F(k)|^2) = NE(|H(r_j,k)|^2). \tag{5}$$

If a signal is obtained from the magnitude of a sum of complex values, each of random phase, this signal will be described by the Rayleigh distribution [15], provided the number of values in the sum is sufficiently large. Therefore, in the limit of large numbers (i.e. large N), the likelihood function describing the magnitude of the signal at any given k will be defined by a Rayleigh distribution:

$$p(|F(k)||\lambda) = \frac{|F(k)|}{\lambda(k)^2}\exp\left(-\frac{|F(k)|^2}{2\lambda(k)^2}\right), \tag{6}$$

where $\lambda^2 = E(|F(k)|^2)/2$. The value of N required for Eq. (6) to hold will depend on the distribution of bubble sizes in the system. For bubbles of a uniform size, $E(|H(r_j,k)|^2) = |H(\bar{r},k)|^2$ and therefore Eq. (6) holds for $N \geqslant 2$. For a bubble size distribution given by a log-normal distribution the value of N required will depend on the parameters of the distribution and an expression similar to Eq. (6) can be derived numerically; for log-normal distributions with $\sigma_r < 0.5\bar{r}$, numerical results show that Eq. (6) holds for realistic experimental values of N (i.e. $N \geqslant 6$).

Eq. (6) defines the likelihood function for the signal as a function of $\bar{r}$ and σ_r. Therefore, if λ^2 is known for all $\bar{r}$ and σ_r, $p(\theta|\hat{y})$ is obtained from Eq. (2), and this can be used to estimate $\theta \equiv \{\bar{r},\sigma_r\}$ which

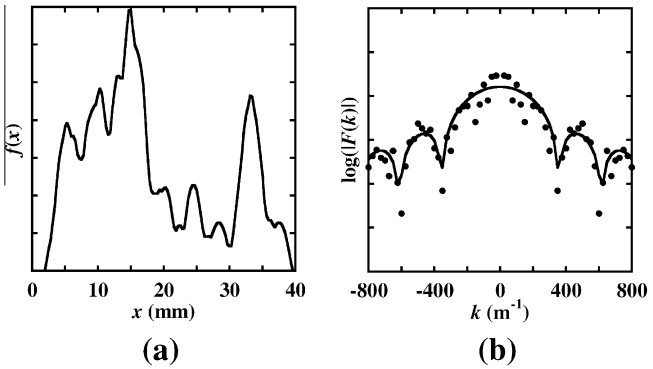

Fig. 1. (a) Plot of the projection onto the x-axis of 30 spheres each of radius 2 mm and (b) (•) the magnitude of $|F(k)|$ and (—) $E(|F(k)|)$ of the discrete Fourier transform of the data shown in (a). The intensity on the vertical axis in (a) is proportional to $\int\int \rho(x,y,z)dydz$. The solid line in (b) is derived from Eqs. (6) and (7).

characterises the bubble size distribution. Assuming gas bubbles in water to be spherical in shape [16] and a size distribution given by a delta function, i.e. $\sigma_r = 0$ such that $r_j = \bar{r}$ for all j, an analytical expression for $H(r,k)$, and therefore λ, is obtained:

$$\lambda^2(r,k) = \frac{N}{2}\left(\frac{\sin(2\pi kr) - 2\pi kr\cos(2\pi kr)}{2\pi^2 k^3}\right)^2. \quad (7)$$

$E(|F(k)|)$, calculated using Eqs. (6) and (7), is shown in Fig. 1b for the simulated data. For more complex shapes or distributions of sizes, a numerical approach is preferable where $E(|H(r_j,k)|^2)$ is obtained by Monte-Carlo simulation.

The validity of the choice of likelihood function given by Eq. (6), was tested by numerically simulating the signal intensity, $|F(k)|$, generated for an image comprising of 10 randomly positioned bubbles each of radius 2 mm. By repeating this simulation many (10^4) times the probability distribution for $|F(k)|$ was obtained. These results are shown in Fig. 2 for $k = 225$ m^{-1} and 525 m^{-1}, and are in good agreement with the theoretical Rayleigh distribution obtained from Eqs. (6) and (7). Similar results were obtained when λ was derived using a numerical simulation. These results suggest that our choice of the likelihood function is appropriate.

3. Results and discussion

The robustness of the Bayesian bubble sizing approach with respect to realistic bubble size distributions was first tested numerically. Bubbles from a predefined size distribution (i.e. known $\bar{r}$ and σ_r) were selected by Monte-Carlo simulation to produce the image $f(x)$, and consequently $F(k)$. Bayes theorem, Eq. (2), was then used to calculate the posterior distribution, from which the parameters $\bar{r}$ and σ_r, and hence the bubble size distribution, were estimated. A simple uninformative prior was used. It was defined as a set of discrete of values evenly spaced within the range 0.15–3.5 mm; the probability of each of the parameter values considered was assumed to be identical. The likelihood was defined by Eqs. (6) and (7). Analysis was performed using 128 data points in k-space. Initially this process was performed for a bubble size distribution given by a delta function, and thus only the mean size ($\bar{r}$) was estimated. The simulation was repeated 20 times with $\bar{r}$ increasing from 0.3 to 3 mm in each subsequent simulation. Fig. 3a shows a plot of the posterior mean $\bar{r}$ for each simulation against the input size in that simulation. The uncertainty in the estimated $\bar{r}$ was calculated from the standard deviation of the posterior distribution for each input $\bar{r}$. The results indicate that for bubbles between 0.3 mm and 3 mm diameter, the method yields excellent estimates of the input bubble size. The root mean squared (rms) error for these data was 0.04 mm. The sensitivity of the measurement to the chosen prior was tested by comparing the estimates of $\bar{r}$ using a prior that was uniform in the logarithm of the bubble size. This was found to change the estimate of the mean size by <1%. It should be noted that the range of bubble size being characterised can be scaled arbitrarily within the limits of the signal-to-noise ratio (SNR) and the physical dimensions of the radiofrequency coil by changing the k-space points sampled. This means that in practice the technique is applicable to measurements where $\bar{r}$ ranges from 30 μm up to 30 mm.

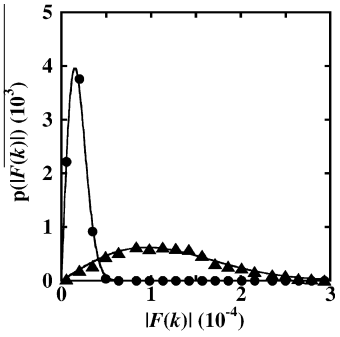

Fig. 2. Plot showing the simulated probability distribution for $|F(k)|$ of 10 bubbles at (▲) $k = 225$ m^{-1} and (•) $k = 525$ m^{-1}. The lines give the theoretical probability distributions as defined by Eq. 6.

The accuracy of estimation of $\bar{r}$ when the bubbles are given by a log-normal distribution (i.e. with non-zero σ_r) is also illustrated in Fig. 3a. The data in Fig. 3a show that the bubble size distribution is estimated with a rms error of 0.1 mm for $\bar{r}$; a similar result was obtained for σ_r. In these simulations, $\sigma_r = 0.15\bar{r}$ in each case. However, by changing the number of data points sampled, larger standard deviations up to at least $\sigma_r = 0.5\bar{r}$ can be measured.

To examine the effect of noise on the estimate of $\bar{r}$ and σ_r, Gaussian noise was added to the complex k-space data. Noise effectively sets a lower bound on the expected signal intensity, thereby reducing some of the information available, particularly at high k-space values. The effect of experimental noise on the estimation of $\bar{r}$ is shown in Fig. 3b and on the estimation of σ_r in Fig. 3c. The rms errors for $\bar{r}$ from these data were 0.1 and 0.4 mm for SNRs of 1000 and 10, respectively, indicating that even in the presence of substantial noise it is possible to estimate the bubble size accurately.

Lastly, the effect of increasing gas fraction was examined. As the gas fraction increases the positions of bubbles become constrained by the location of other nearby bubbles thereby introducing ordering into the locations of bubbles. The effect of this exclusion process on the estimated size distribution was tested by numerically generating a set of data $|F(k)|$ where bubbles were sequentially added such that the position of new bubbles was constrained by the locations of previously placed bubbles. This was achieved by choosing the location of new bubbles using a probability density function governed by the unoccupied cross-sectional area of a column remaining at each vertical position x along the length of the column. This probability distribution is described by:

$$p_{x_{c,n}}(x|D_c,\{x_c\}) \propto \frac{\pi D_c^2}{4} - \sum_{j=1}^{n-1}\begin{cases}\pi\left(r_j^2 - (x-x_{cj})^2\right) & \text{if } |x-x_{cj}| \leqslant r_j \\ 0 & \text{if } |x-x_{cj}| > r_j\end{cases}, \quad (8)$$

where $p_{x_{c,n}}$ is the probability of finding the nth bubble centred at any point x, x_{cj} is the location of the centre of the jth bubble, D_c is the diameter of the containing column and r_j is the diameter of the jth bubble. Any point x would be rejected if it would result in the volume of bubbles in a given cross sectional slice exceeding the volume of that slice. A new point x would then be chosen using Eq. (8). An estimate of $\bar{r}$ was then obtained using the approach outlined above for gas fractions from 1% up to 60%. Over this range of gas fractions using a SNR of 1000 with $\bar{r}$ set to 1.6 mm and σ_r set to 0.1 mm, the mean bubble size was estimated accurately for gas fractions up to 50%, as shown in Fig. 4. At gas fractions in excess of 50%, the measurement begins to deteriorate, however we note that the bubble flow will likely transition to slug flow at a gas fraction below 50%. This confirms that the technique is valid for measurements of bubble size distributions up to the highest gas fractions at which gas bubbles will exist.

To test our approach experimentally, $\bar{r}$ and σ_r were measured on a system with a low gas fraction using both an optical technique and the MR technique proposed in this work. The apparatus consisted of a 31 mm inner diameter column filled with deionised water containing 0.1 mg ml^{-1} sodium dodecyl sulphate to minimise bubble coalescence and 16.8 mM dysprosium chloride to reduce the water relaxation time and minimise susceptibility differences between the water and air. Gas bubbles were

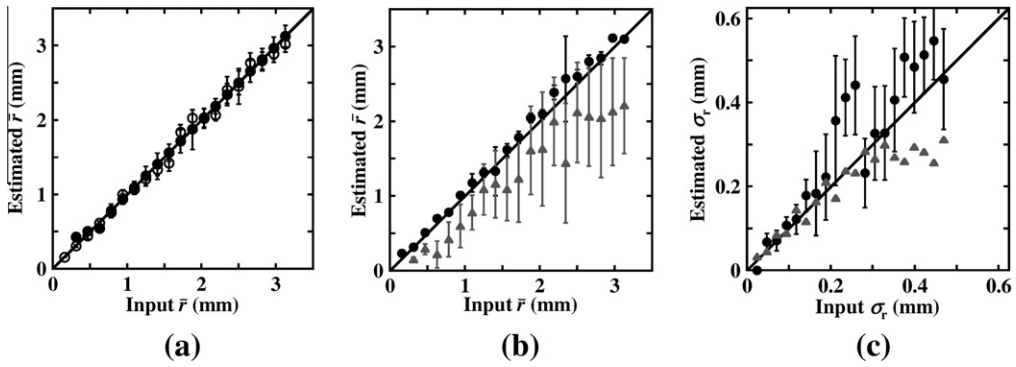

Fig. 3. (a) Estimated $\bar{r}$, as a function of the input $\bar{r}$ for (•) delta function and (○) log-normal bubble size distributions in the absence of noise. (b) Estimated $\bar{r}$ and (c) estimated σ_r for log-normal bubble size distributions in the presence of added Gaussian noise where the SNR was (•) 1000 and (▲) 10. Each simulation contained 10 bubbles selected from the appropriate bubble size distribution and the solid lines describe the desired trend, i.e. $y = x$. The error bars are given by the standard deviation of the posterior distribution.

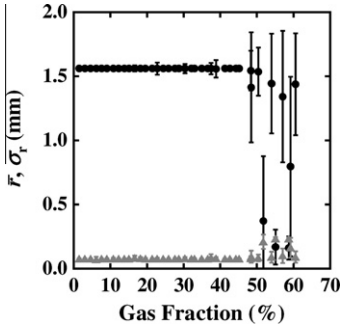

Fig. 4. Simulations illustrating the effect of ordering arising from dense concentrations of bubbles. The parameters (•) $\bar{r}$ and (▲) σ_r were estimated for simulations at increasing gas fraction with $\bar{r} = 1.6$ mm and $\sigma_r = 0.1$ mm. The sizing is shown to be robust up to a gas fraction of at least 50%. The effect of increasing gas fraction was simulated according to Eq. (8).

introduced using either a porous stone (distributor 1) or porous rubber (distributor 2) gas-sparger. To compare bubble size distributions at low gas fraction, which could be characterised using both MR and optical measurements, a gas flow rate of 100 ml min^{-1} was used. At this gas flow rate the gas fraction in the system was ~2% with both distributors. The MR technique was also demonstrated at a higher gas fraction using a flow rate of 1000 ml min^{-1}, giving a gas fraction of ~15%. Photographs of the system were obtained using a Canon Powershot A630 digital camera. MR measurements were performed on a Bruker AV400 spectrometer with a 38 mm imaging coil.

The Bayesian approach eliminates the requirement of conventional image acquisition that every point in k-space be sampled with the same bubbles located at the same positions. Instead we require only that all samples are obtained from the same bubble size distribution, i.e. the distribution of bubble sizes are governed by the same $\bar{r}$ and σ_r. Therefore, data were acquired using a single point imaging (SPI) protocol [17] which had the advantages of minimising the effects of velocity attenuation on the signal and allowing selective acquisition of the data from the most appropriate positions in k-space, thereby improving the accuracy of the measurement. The experiment was performed in two steps: (1) a single point was acquired to determine the gas fraction at the given gas flow rate, then (2) 128 data points were acquired for k-space points ranging from -2270 m^{-1} to 2270 m^{-1}, but excluding points for $|k| \leqslant 133$ m^{-1}. The excluded points are dominated by the low spatial frequency information and therefore contain little information about the bubble size distribution. This approach is analogous to that of Barrall et al. [12], though has the advantage that the signal for $|F(k)|$ at large k can be amplified further without saturating the receiver since high intensity signals at low k are not measured. This increases the SNR for those points measured, and therefore improves the accuracy of the estimate of $\bar{r}$ and σ_r.

Fig. 5a and b shows two photographs of the bubbles in the column using the two gas distributors. As seen in Fig. 5, distributor 2 produces larger bubbles than distributor 1. As the gas fraction in these systems was very low (~2%), the bubble size distribution could be measured directly from the photographs. These are shown by the solid lines in Fig. 5c. For the optical measurement and analysis >50 bubbles were measured. The dashed lines in Fig. 5c show the bubble size distribution calculated using the Bayesian approach outlined in this paper to obtain the parameters $\bar{r}$ and σ_r of a log-normal distribution of bubble sizes. The function λ^2 was obtained from a Monte-Carlo simulation of a log-normal bubble size distribution. The bubble size distributions measured for each system using the optical and MR techniques were in excellent agreement. The Bayesian approach is equally valid for both low

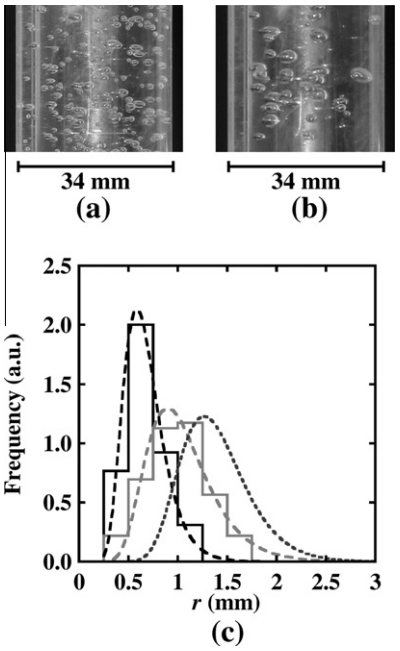

Fig. 5. Photographs of a swarm of gas bubbles obtained using (a) distributor 1 and (b) distributor 2 at a gas fraction of ~2% in each case. (c) Comparison of the size distribution obtained in these systems using distributor 1 (black) and distributor 2 (grey) from both the optical (solid lines) and MR (dashed lines) techniques. MR measurements were also taken at a gas fraction of ~15% using distributor 2 (dotted line) where the optical technique could not be used.

and high gas fraction systems and therefore can be used in systems where optical techniques cannot. This is demonstrated in Fig. 5 by the measurement of the bubble size distribution at a gas fraction of ~15%, well beyond that which can be measured optically. The mean bubble size was seen to increase, as would be expected due to the increased probability of bubble coalescence in a dense bubble swarm.

4. Conclusions

In this paper a method for measuring the size distribution of gas bubbles has been developed based on Bayesian analysis of MR data. The method is demonstrated to provide measurements of bubble size distribution in gas–liquid flows which cannot be measured using other MR approaches, and at gas fractions in excess of those that can be studied optically.

References

[1] P. Mansfield, Multi-planar image formation using NMR spin echoes, J. Phys. C 10 (1977) 55–58.
[2] J. Hennig, A. Nauerth, H. Friedburg, RARE imaging: a fast imaging method for clinical MR, Magn. Reson. Med. 3 (1986) 823–833.
[3] A. Haase, J. Frahm, D. Matthaei, W. Hanicke, K. Merboldt, FLASH imaging. Rapid NMR imaging using low flip-angle pulses, J. Magn. Reson. 67 (1986) 258–266.
[4] S. Saxena, D. Patel, D. Smith, J. Ruether, An assessment of experimental techniques for the measurement of bubble size in a bubble slurry reactor as applied to indirect coal liquefaction, Chem. Eng. Commun. 63 (1988) 87–127.
[5] A. Cartellier, J.L. Achard, Local phase detection probes in fluid/fluid two-phase flows, Rev. Sci. Instrum. 62 (1991) 279–303.
[6] R. Mudde, J. Groen, H. Van Den Akker, Application of LDA to bubbly flows, Nucl. Eng. Des. 184 (1998) 329–338.
[7] G.L. Bretthorst, C. Hung, D.A. D'Avignon, J.J.H. Ackerman, Bayesian analysis of time-domain magnetic resonance signals, J. Magn. Reson. 79 (1988) 369–376.
[8] G.L. Bretthorst, W.C. Hutton, J.R. Garbow, J.J.H. Ackerman, Exponential parameter estimation (in NMR) ssing Bayesian probability theory, Concepts Magn. Reson. A 27A (2005) 55–63.
[9] D. Xing, S.J. Gibbs, J.A. Derbyshire, E.J. Fordham, T.A. Carpenter, L.D. Hall, Bayesian analysis for quantitative NMR flow and diffusion imaging, J. Magn. Reson. B 106 (1995) 1–9.
[10] R.W. Wise, B. Newling, A.R.C. Gates, D. Xing, T.A. Carpenter, L.D. Hall, Measurement of pulsatile flow using MRI and a Bayesian technique of probability analysis, Magn. Reson. Imag. 14 (1996) 173–185.
[11] R. Gonzalez, R. Woods, Digital Image Processing, Prentice Hall, New Jersey, 2008.
[12] G.A. Barrall, L. Frydman, G.C. Chingas, NMR diffraction and spatial statistics of stationary systems, Science 255 (1992) 714–717.
[13] P. Callaghan, Principles of Nuclear Magnetic Resonance Microscopy, Clarendon Press, Oxford, 1991.
[14] W. Deckwer, Bubble Column Reactors, Wiley, Chichester, 1992.
[15] A. Cardenas-Blanco, C. Tejos, P. Irarrazaval, I. Cameron, Noise in magnitude magnetic resonance images, Concepts Magn. Reson. A 32A (2008) 409–416.
[16] R. Clift, J. Grace, M. Weber, Bubbles, Drops, and Particles, Academic Press, New York, 1978.
[17] S. Emid, J. Creyghton, High resolution NMR imaging in solids, Physica B 128 (1985) 81–83.